The canonical non-homologous end joining factor XLF promotes chromosomal deletion rearrangements in human cells

Received for publication, August 2, 2019, and in revised form, November 20, 2019 Published, Papers in Press, November 21, 2019, DOI 10.1074/jbc.RA119.010421

Ragini Bhargava[‡§], **Felicia Wednesday Lopezcolorado**[‡], **L. Jillianne Tsai**[‡§], **and Jeremy M. Stark**[‡§1]

From the [‡]*Department of Cancer Genetics and Epigenetics and* [§]*Irell and Manella Graduate School of Biological Sciences, Beckman Research Institute of the City of Hope, Duarte, California 91010*

Edited by Patrick Sung

Clastogen exposure can result in chromosomal rearrangements, including large deletions and inversions that are associated with cancer development. To examine such rearrangements in human cells, here we developed a reporter assay based on endogenous genes on chromosome 12. Using the RNA-guided nuclease Cas9, we induced two DNA double-strand breaks, one each in the *GAPDH* and *CD4* genes, that caused a deletion rearrangement leading to *CD4* expression from the *GAPDH* promoter. We observed that this *GAPDH–CD4* deletion rearrangement activates CD4+ cells that can be readily detected by flow cytometry. Similarly, double-strand breaks in the *LPCAT3* and *CD4* genes induced an *LPCAT3–CD4* inversion rearrangement resulting in *CD4* expression. Studying the *GAPDH–CD4* deletion rearrangement in multiple cell lines, we found that the canonical non-homologous end joining (C-NHEJ) factor XLF promotes these rearrangements. Junction analysis uncovered that the relative contribution of C-NHEJ appears lower in U2OS than in HEK293 and A549 cells. Furthermore, an ATM kinase inhibitor increased C-NHEJ-mediated rearrangements only in U2OS cells. We also found that an XLF residue that is critical for an interaction with the C-NHEJ factor X-ray repair cross-complementing 4 (XRCC4), and XRCC4 itself are each important for promoting both this deletion rearrangement and end joining without insertion/deletion mutations. In summary, a reporter assay based on endogenous genes on chromosome 12 reveals that XLF-dependent C-NHEJ promotes deletion rearrangements in human cells and that cell type–specific differences in the contribution of C-NHEJ and ATM kinase inhibition influence these rearrangements.

Chromosomal DNA double-strand breaks (DSBs)[2] are the therapeutically effective lesion for cancer radiotherapy, and, conversely, DSBs can be an initiating event for cancer-associated mutations and chromosomal rearrangements (1, 2). Indeed, end joining (EJ) repair of DSBs that causes insertion/deletion (indel) mutations or chromosomal rearrangements could result in the loss of tumor suppressor genes or the formation of oncogenic fusion genes (3–7). For example, deletion rearrangements have been observed in a wide-array of tumor types, and 0.5 megabase pairs (Mbp) was the average size of somatic deletions found in a set of more than 700 cancer lines (6). As another example, radiation-associated secondary malignancies carry a relatively high frequency of deletion mutations with microhomology at the junctions and balanced inversion rearrangements (3). Thus, characterizing the mechanisms of DSB repair via EJ is critical for developing strategies to improve cancer radiotherapy and to understand cancer etiology (2, 8).

Chromosomal EJ repair can occur by either canonical non-homologous EJ (C-NHEJ) or alternative EJ (Alt-EJ) (9–12). The C-NHEJ pathway involves the core factors KU (KU70/KU80), DNA-PKcs, XRCC4, XLF, and DNA ligase IV (LIG4) (10, 11). However, in the absence of these C-NHEJ factors, chromosomal EJ remains relatively proficient, albeit more prone to deletion mutations with microhomology at the junctions (13–20). Such repair is proscribed to the Alt-EJ pathway, which involves DNA polymerase θ (POLQ), among other factors (13–20). Consistent with a partially redundant role in EJ, combined loss of POLQ and the C-NHEJ factor KU80 causes striking radiosensitivity (21).

The relative contribution of C-NHEJ and Alt-EJ to the etiology of chromosomal rearrangements has remained unclear. Cancer-associated chromosomal rearrangements often show evidence of microhomology, which could reflect a substantial contribution of Alt-EJ (5, 7). However, rearrangements without microhomology are also readily detected (7). Furthermore, although microhomology is not required for C-NHEJ, this pathway can nevertheless mediate these repair events (22). The relative contributions of these pathways to rearrangement formation could also be specific to individual cell types and/or species. Indeed, experiments monitoring rearrangement frequencies induced by targeted DSBs (*e.g.* I-SceI or the RNA-guided nuclease Cas9) have revealed such distinctions. Specifically, in mouse embryonic stem cells (mESCs), chromosomal translocations are relatively independent of the C-NHEJ pathway (23). In contrast, human cells appear to show a greater role for C-NHEJ in translocation formation, as detected using PCR-based assays (24).

This work was supported by NCI, National Institutes of Health Grants R01CA197506 (to J. M. S.) and P30CA33572 (to City of Hope Core Facilities). The authors declare that they have no conflicts of interest with the contents of this article. The content is solely the responsibility of the authors and does not necessarily represent the official views of the National Institutes of Health.

[1] To whom correspondence should be addressed: 1500 E. Duarte Rd., Duarte, CA 91010. Tel.: 626-218-6436; Fax: 626-301-8892; E-mail: jstark@coh.org.

[2] The abbreviations used are: DSB, double-strand break; EJ, end joining; indel, insertion/deletion; Alt-EJ, alternative EJ; Mbp, megabase pair; C-NHEJ, canonical non-homologous EJ; mESC, mouse embryonic stem cells; sgRNA, single-guide RNA; 3XF, 3×FLAG immunotag; ATMi, ATM kinase inhibitor KU-55933; ATMi-2, ATM kinase inhibitor KU-60019; DNAPKi, small molecule DNA-PKcs kinase inhibitor NU7441; EV, empty vector.

Apart from cell type *per se*, DNA damage response signaling pathways appear to affect the contribution of C-NHEJ *versus* Alt-EJ in rearrangement formation. Namely, a prior study from our laboratory found that ATM inhibits chromosomal rearrangements mediated by C-NHEJ in mESCs, using an assay for a 0.4 Mbp deletion (25). In particular, ATM appears important to inhibit a rearrangement junction type that is a hallmark of C-NHEJ: EJ of blunt DSBs without indels, *i.e.* No Indel EJ (25, 26). We have sought to perform an analogous set of experiments in human cells. Thus, we present an assay for a deletion rearrangement in human cells that uses endogenous genes and describe the influence of XLF and inhibition of the ATM kinase on this rearrangement.

Results

Reporter assay for chromosomal rearrangements in human cells based on endogenous genes, with CD4 expression as the readout

We have sought to understand the mechanisms of chromosomal rearrangement formation in human cells via a reporter assay that uses endogenous genes. For this, we chose the *CD4* gene on human chromosome 12, because expression of this gene is largely restricted to cells in the immune system (27, 28). Furthermore, expression of this protein is readily detected by flow cytometry using commercial antibodies. Indeed, EJ reporter cassettes have been previously developed using the *CD4* gene as the readout (17, 29). Thus, we posited that rearrangements that link an active promoter with the *CD4* coding region would lead to CD4 expression that could be detected by flow cytometry. To detect deletions, we used the promoter for *GAPDH*, which is in the same orientation, 0.25 Mbp upstream of *CD4* (Fig. 1*a*). To detect inversions, we used the promoter for *LPCAT3*, which is in the opposite orientation, 0.23 Mbp downstream of *CD4* (Fig. 1*a*). These locations are based on Genome Reference Consortium Human Build 38 (assembly accession reference: GCA_000001405.27).

We first tested this approach in the human osteosarcoma cell line U2OS, which is a common cell line for studies of the DNA damage response, as these cells retain intact cell cycle checkpoints (26, 30–32). These cells also use the alternative lengthening of telomere pathway of telomere maintenance, and hence are also a model system to examine this aspect of the DNA damage response (33). We used a version of this cell line that is stably transfected with pFRT/lacZeo (U2OS Flp-In T-Rex) (26, 30), which is relevant for another assay described below (*i.e.* integration of the EJ7-GFP reporter). With this cell line, we found that expressing Cas9 with sgRNAs targeting *GAPDH* and *CD4*, or *LPCAT3* and *CD4*, substantially induces CD4+ cells (Fig. 1*b*). We isolated CD4+ U2OS cells via flow cytometry and used PCR to confirm the expected rearrangement (Fig. 1*a*). We also expressed Cas9 and the individual sgRNAs, and found that targeting *GAPDH* and *LPCAT3* alone did not induce CD4+ cells (Fig. 1*b*). Finally, expressing Cas9 and the sgRNA targeting *CD4* alone induced CD4+ cells above background levels, but the frequency of CD4+ cells was much lower than that of the rearrangements (Fig. 1, *b* and *c*).

Note that this assay relies on determining the percentage of cells that are CD4+. In contrast, this analysis does not provide a measure of how many chromosomes per cell have undergone the rearrangement, because each cell likely has multiple copies of chromosome 12 (34). Namely, a cell with multiple copies of this region of chromosome 12 likely has a greater probability of forming the rearrangement, and hence becoming CD4+, than a cell that has fewer copies of this chromosomal region. Thus, this potential effect of chromosome 12 ploidy on this assay system should be considered when comparing the overall frequencies of CD4+ cells between different cell types.

We then examined the feasibility of this approach in three other cell lines: the A549 lung cancer cell line (35), an adenovirus immortalized human embryonic kidney cell line that is stably transfected with pFRT/lacZeo (HEK293 Flp-In T-Rex) (36), and an SV40 immortalized human fibroblast cell line (GM00637, Coriell). In all experiments, CD4+ frequencies are normalized to transfection efficiency using a parallel transfection with a GFP expression vector (Fig. 1*c*). Beginning with the *GAPDH–CD4* deletion rearrangement, in each of these cell lines, we found that targeting pairs of DSBs to *GAPDH* and *CD4* caused a significant induction of CD4+ cells, compared with targeting a DSB to *CD4* alone (Fig. 1*c*). Regarding the *LPCAT3–CD4* inversion rearrangement, we found that targeting DSBs to *LPCAT3* and *CD4* in A549, HEK293, and GM00637 cells did not cause a significant induction of CD4+ cells, compared with targeting a DSB to *CD4* alone (Fig. 1*c*). In summary, targeting Cas9-induced DSBs to specific sites on chromosome 12 in several human cell lines is sufficient to induce chromosomal rearrangements that can be detected through CD4 expression. However, detection of the *GAPDH–CD4* deletion rearrangement was more robust in each cell type, compared with the *LPCAT3–CD4* inversion rearrangement (Fig. 1*c*). Indeed, the inversion rearrangement was only significantly induced in U2OS cells, compared with targeting a DSB to CD4 alone.

The C-NHEJ factor XLF promotes deletion rearrangements in both U2OS and HEK293, whereas an ATM kinase inhibitor causes an increase in deletion rearrangements only in U2OS cells

Using the *GAPDH–CD4* rearrangement assay, we sought to examine the influence of XLF on deletion rearrangements. We examined XLF, because this factor has emerged as a key stabilizing factor in the C-NHEJ complex (26, 37–39). Thus, we used Cas9 and a sgRNA targeting *XLF* (40) to generate knockout cell lines (*XLF-KO*) for both U2OS and HEK293 cells (Fig. 2*a*). We compared *XLF-KO* cells to both the parental cell line and to cells with expression of XLF WT (Fig. 2*a*). For the latter, an expression vector for XLF WT with an N-terminal 3×FLAG (3XF) immunotag is included in the transfection with the Cas9/sgRNA plasmids. From these experiments, both U2OS and HEK293 *XLF-KO* cells showed a significantly lower frequency of the deletion rearrangement *versus* the parental cell line (Fig. 2*b*). Furthermore, expression of XLF WT in the *XLF-KO* cells restored the rearrangement frequency to near the levels of the parental cells (Fig. 2*b*). Thus, XLF promotes deletion rearrangements in both HEK293 and U2OS cells.

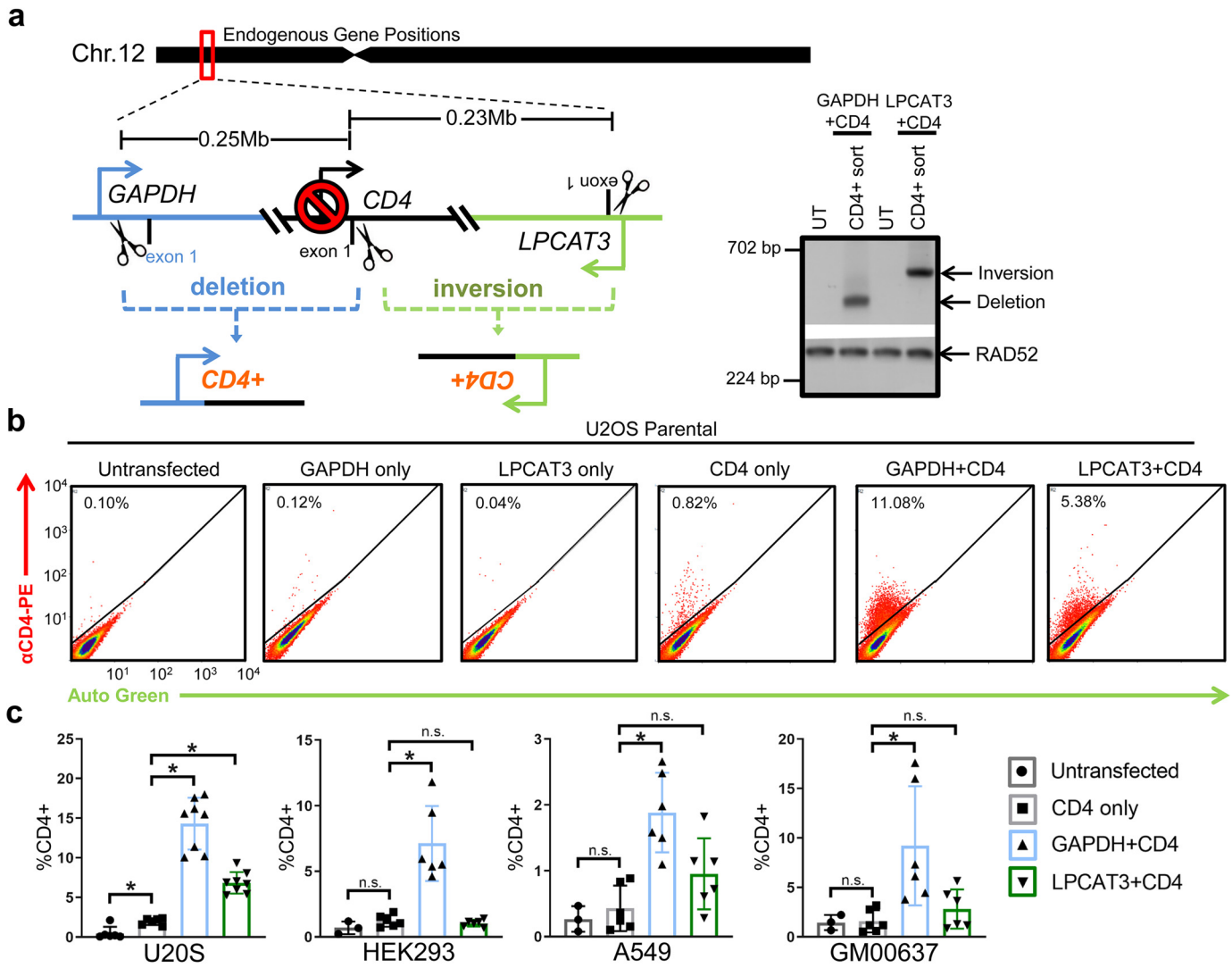

Figure 1. A reporter assay for chromosomal rearrangements in human cells that uses the endogenous *CD4* gene. *a*, shown is a schematic for examining deletion and inversion rearrangements in human cells using endogenous genes on chromosome 12. Relative positions are based on Genome Reference Consortium Human Build 38. *Scissors* indicate sgRNA target sites for the Cas9 nuclease. Also shown are PCR amplification products from sorted CD4+ U2OS cells to detect the *GAPDH–CD4* deletion rearrangement and the *LPCAT3–CD4* inversion rearrangement, with an amplicon of *RAD52* as a control. Amplification products from untransfected (*UT*) cells are also shown. *b*, shown are representative flow cytometry plots for U2OS cells that were either untransfected (*UT*), or transfected with expression plasmids for Cas9/sgRNAs targeting the *GADPH*, *LPCAT3*, or *CD4* locus only, or Cas9/sgRNAs targeting the *GAPDH* and *CD4* loci (GAPDH plus CD4) or the *LPCAT3* and *CD4* loci (LPCAT3 plus CD4). *c*, shown is the frequency of CD4+ cells, normalized to transfection efficiency with parallel transfections with a GFP expression plasmid, for four different human cell lines. Shown is the mean with S.D. *, $p \leq 0.04$, using an unpaired *t* test with Holm-Sidak correction; *ns*, not significant. $n \geq 6$ for U2OS, and $n \geq 3$ for HEK293, A549, and GM00637 cells.

In parallel with the above experiments, we also examined the effect of treating cells with a small molecule inhibitor of the ATM kinase KU-55933 (ATMi) (41), because a prior study from our laboratory found that ATMi treatment of mESCs causes an increase in deletion rearrangements in a manner that depends on several C-NHEJ factors, including XLF (25). Notably, the transfections without ATMi were treated with the vehicle used for ATMi (*i.e.* DMSO). From these experiments, we found that ATMi treatment of U2OS cells caused an increase in the frequency of the *GAPDH–CD4* deletion rearrangement in parental cells (Fig. 2*b*), but not the *XLF-KO* cells, unless these cells were complemented with the XLF WT expression vector (Fig. 2*b*). In contrast, ATMi treatment failed to cause an increase in the frequency of deletion rearrangements in HEK293 cells, irrespective of the presence of XLF. Thus, ATM kinase activity appears important to suppress XLF-dependent deletion rearrangements in U2OS cells.

We also tested other small molecule kinase inhibitors to evaluate the specificity of the effect of ATMi treatment in U2OS cells. For one, we tested a second ATM inhibitor, KU-60019 (ATMi-2) (42). We also tested a kinase inhibitor of DNA-PKcs, NU7441 (DNAPKi) (43). ATM and DNA-PKcs are both phosphoinositide three kinase–related protein kinases (44). DNA-PKcs associates with KU to form the DNA-dependent protein kinase, which catalyzes several autophosphorylation events on DNA-PKcs (45). We examined the effect of each of these kinase inhibitors on the frequency of the *GAPDH–CD4* rearrangement in U2OS cells. We found that treatment with KU-60019 (ATMi-2) caused a significant increase in the frequency of the *GAPDH–CD4* rearrangement, similar to treatment with

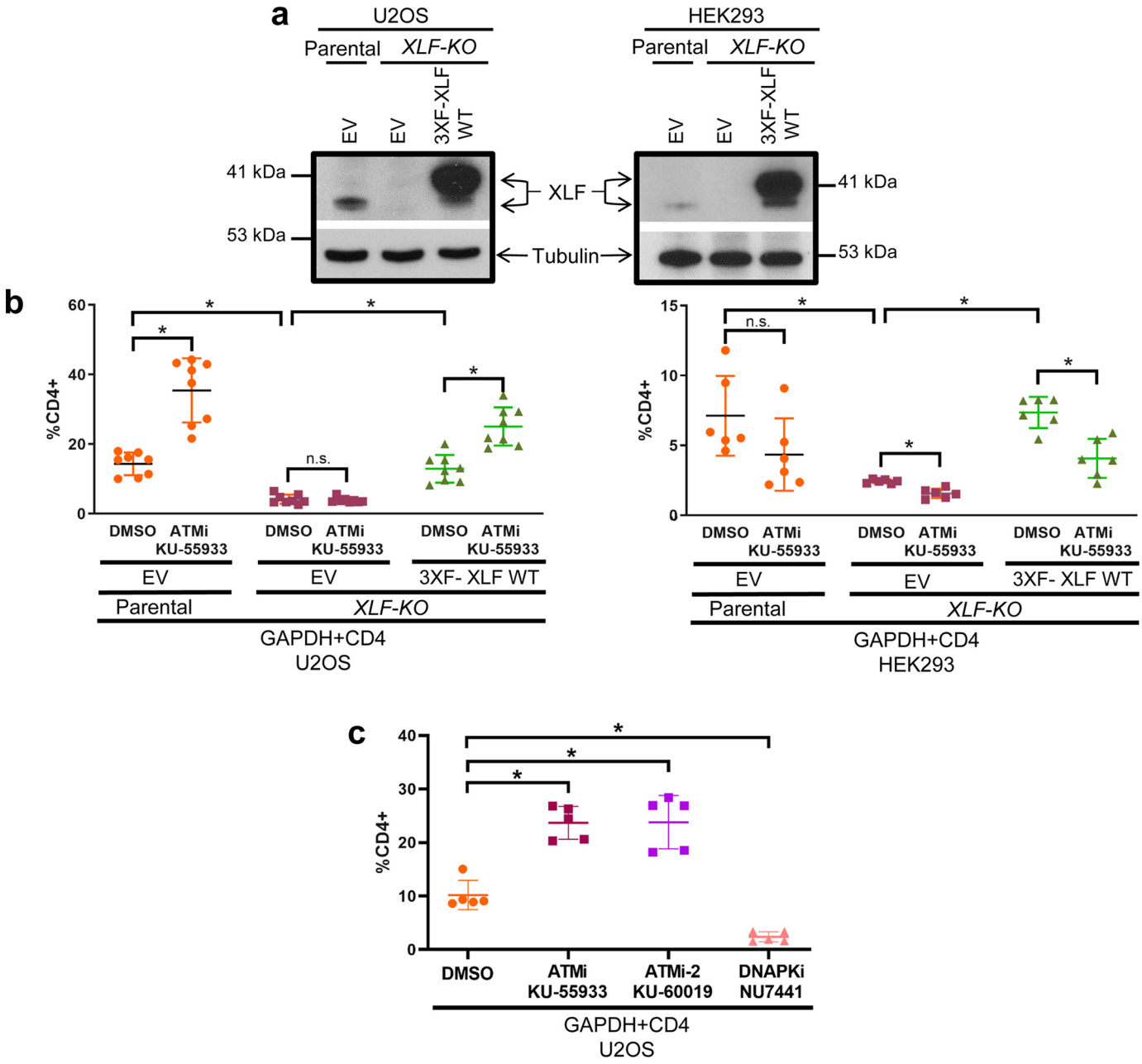

Figure 2. Examining the influence of XLF-deficiency and ATMi treatment on deletion rearrangements in U2OS and HEK293 cells. *a*, shown are immunoblots for XLF from U2OS and HEK293 parental cells, and *XLF-KO* cell lines, transfected with either a control EV or a 3×FLAG-tagged XLF WT (3XF–XLF WT) expression vector. *b*, shown is the percentage of CD4+ cells in parental or *XLF-KO* U2OS and HEK293 cells transfected with the GAPDH and CD4 sgRNA/Cas9 expression vectors, along with either a control vector (EV) or a 3XF–XLF WT vector in the presence of either the ATMi or vehicle (DMSO), normalized to transfection efficiency as in Fig. 1*c*. *n.s.*, not significant. Shown is the mean with S.D. *, $p \leq 0.005$ ($n = 8$ for U2OS cells, and $n = 6$ for HEK293 cells), using an unpaired *t* test with Holm-Sidak correction. *c*, shown is the percentage of CD4+ cells in U2OS cells transfected with the GAPDH and CD4 sgRNA/Cas9 expression vectors and treated with different small molecule kinase inhibitors: KU-55933 (ATMi), another ATM kinase inhibitor KU-60019 (ATMi-2), and the DNA-PKcs inhibitor NU7441 (DNAPKi). The control sample was treated with vehicle (DMSO), and CD4+ frequencies were normalized to transfection efficiency as in Fig. 1*c*. Shown is the mean with S.D. *, $p \leq 0.001$ ($n = 5$), using an unpaired *t* test with Holm-Sidak correction.

KU-55933 (ATMi) (Fig. 2*c*). In contrast, treatment with NU7441 (DNAPKi) caused a substantial reduction in the frequency of the *GAPDH–CD4* rearrangement (Fig. 2*c*). The finding with DNAPKi is consistent with a key role for DNA-PKcs kinase activity for C-NHEJ (45, 46).

Influence of cell type, XLF, and ATMi treatment on rearrangement junctions

We then sought to examine how XLF disruption and ATMi treatment affected rearrangement junctions in both U2OS and HEK293 cells, because junction patterns can provide insight into the EJ pathways that mediate the rearrangements. For this, we performed the *GAPDH–CD4* rearrangement assay described above, isolated the CD4+ cells by flow cytometry sorting, amplified the *GAPDH–CD4* rearrangement junction, and examined the amplicons by deep sequencing (Fig. 3*a*). For each condition, we examined amplicons from three independent transfections (*i.e.* biological replicates). We determined the frequency of distinct junction types for each amplicon, and

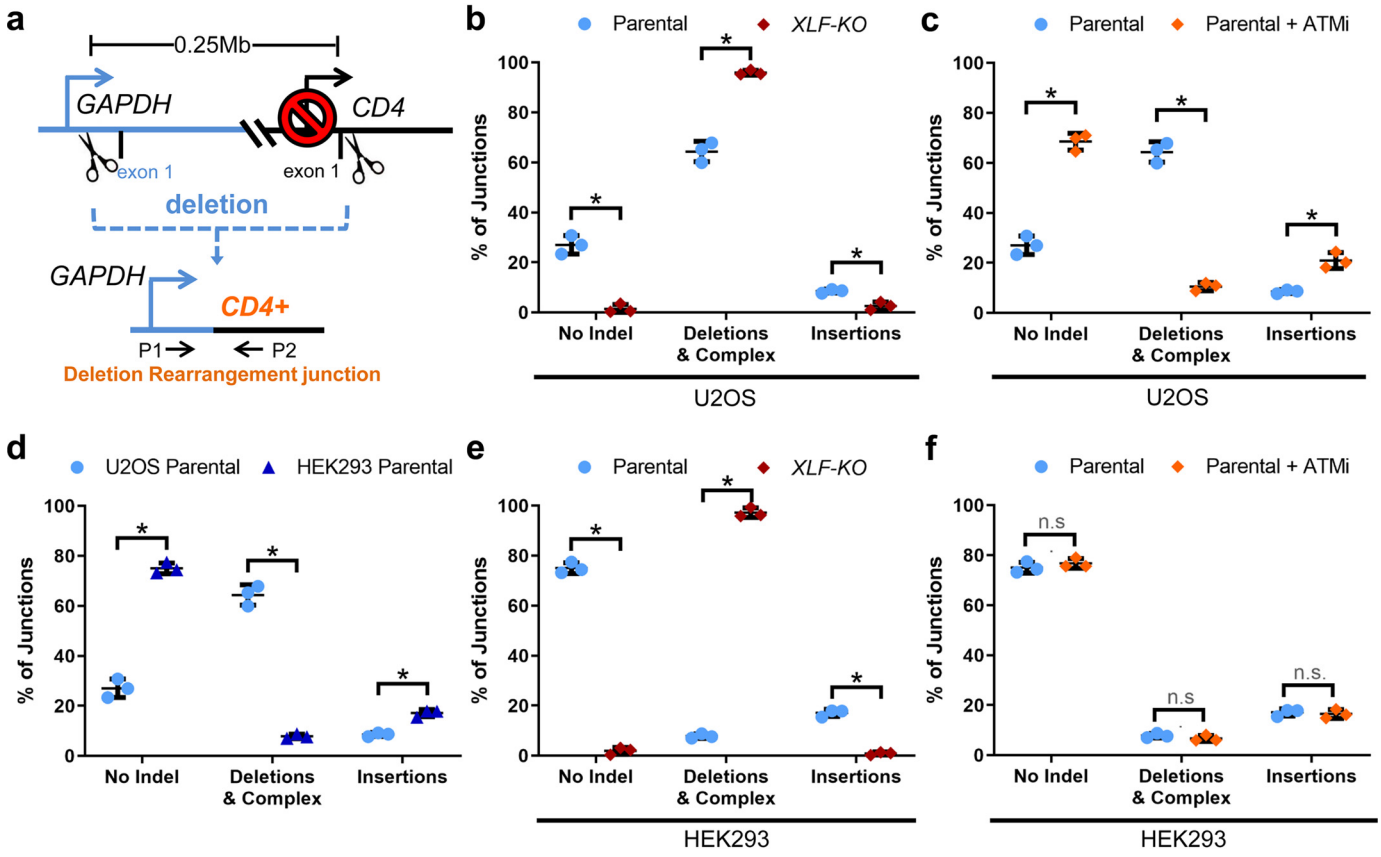

Figure 3. Amplicon deep sequencing analysis of the *GAPDH-CD4* deletion rearrangement junction in U2OS and HEK293 cells, along with effects of XLF-deficiency and ATMi treatment. *a*, shown is a schematic of the *GAPDH–CD4* deletion rearrangement, which gives rise to CD4+ cells. Primers P1 and P2 are used to amplify the rearrangement junction, and the amplicons were used for deep sequencing. All transfections for this analysis were treated with either ATMi (KU-55933) or vehicle (DMSO) for 3 days. *b*, comparison of U2OS parental *versus* U2OS *XLF-KO* junctions. Shown are indel types classified into three categories: No Indel (EJ without any insertions or deletions at the rearrangement junction), insertions (addition of nucleotides at the rearrangement junctions), or deletions and complex (loss of nucleotides at the rearrangement junction, with or without the addition of nucleotides). $n = 3$ amplicons from independent biological replicates. Shown is the mean with S.D. *, $p < 0.003$, *n.s.*, not significant., using an unpaired *t* test with Holm-Sidak correction. *c*, U2OS parental (DMSO) *versus* ATMi junctions. Analysis and statistics as in (*b*). *d*, U2OS parental *versus* HEK293 parental junctions. Analysis and statistics as in (*b*). *e*, HEK293 parental *versus XLF-KO* junctions. Analysis and statistics as in (*b*). *f*, HEK293 parental (DMSO) *versus* ATMi junctions. Analysis and statistics as in (*b*). The U2OS and HEK293 parental junctions are repeated in the different panels to facilitate the various comparisons.

then calculated the mean/S.D. of these frequencies from the three biological replicates. For this analysis, we categorized the junctions into three types: 1) rearrangements without insertion or deletion mutations at the edges of the two Cas9-induced DSBs (*i.e.* No Indel), 2) insertions, and 3) deletions and complex junctions. Regarding the last, complex junctions involve deletions with inserted nucleotides and/or mutations at the junction.

Beginning with U2OS cells, each of these three junction types is readily detectable: 27% No Indel, 8.5% insertions, and 64.4% deletions and complex junctions (Fig. 3*b*). In contrast, the U2OS *XLF-KO* cells show a marked reduction of the No Indel (1.4%) and insertion (2.6%) junction types, and an increase in deletions and complex junctions (96%) (Fig. 3*b*). Thus, XLF is important for the No Indel and insertion junction types. Conversely, U2OS cells treated with ATMi showed a significant increase in the No Indel and insertion junction types (68.5 and 20.9%, respectively), and a decrease in deletions and complex junctions (10.5%) (Fig. 3*c*). Accordingly, ATMi treatment caused an increase in the junction types that are promoted by XLF, which supports the notion that ATM kinase activity is important to suppress XLF-mediated rearrangements.

With HEK293 cells, we found that compared with U2OS cells, these cells show a substantial frequency of the No Indel junction type (75%, 2.7-fold higher than U2OS), an increase in the insertion junction types (17%, 2-fold greater than U2OS), along with a marked reduction in deletions and complex junction types (7.8%, 8.2-fold lower than U2OS) (Fig. 3*d*). In contrast, the HEK293 *XLF-KO* cells show a marked reduction in the No Indel and insertion junction types (1.92 and 0.9%, respectively), as we found with the U2OS *XLF-KO* cells (Fig. 3*e*). Finally, ATMi treatment in HEK293 cells did not obviously affect the types of junctions (Fig. 3*f*).

In summary, XLF is required for the No Indel and insertion junction types in both HEK293 and U2OS cells. Furthermore, we found distinctions among the junction patterns between these cell lines. Namely, HEK293 cells show an increase in the XLF-dependent junction types (No Indel and insertions), compared with U2OS cells.

We then examined microhomology use in the deletion mutations. For this, we isolated all sequences that represented ≥0.25% of the total deletions or complex junctions per amplicon and then determined the microhomology usage for each of the simple deletion sequences. It is not possible to assign

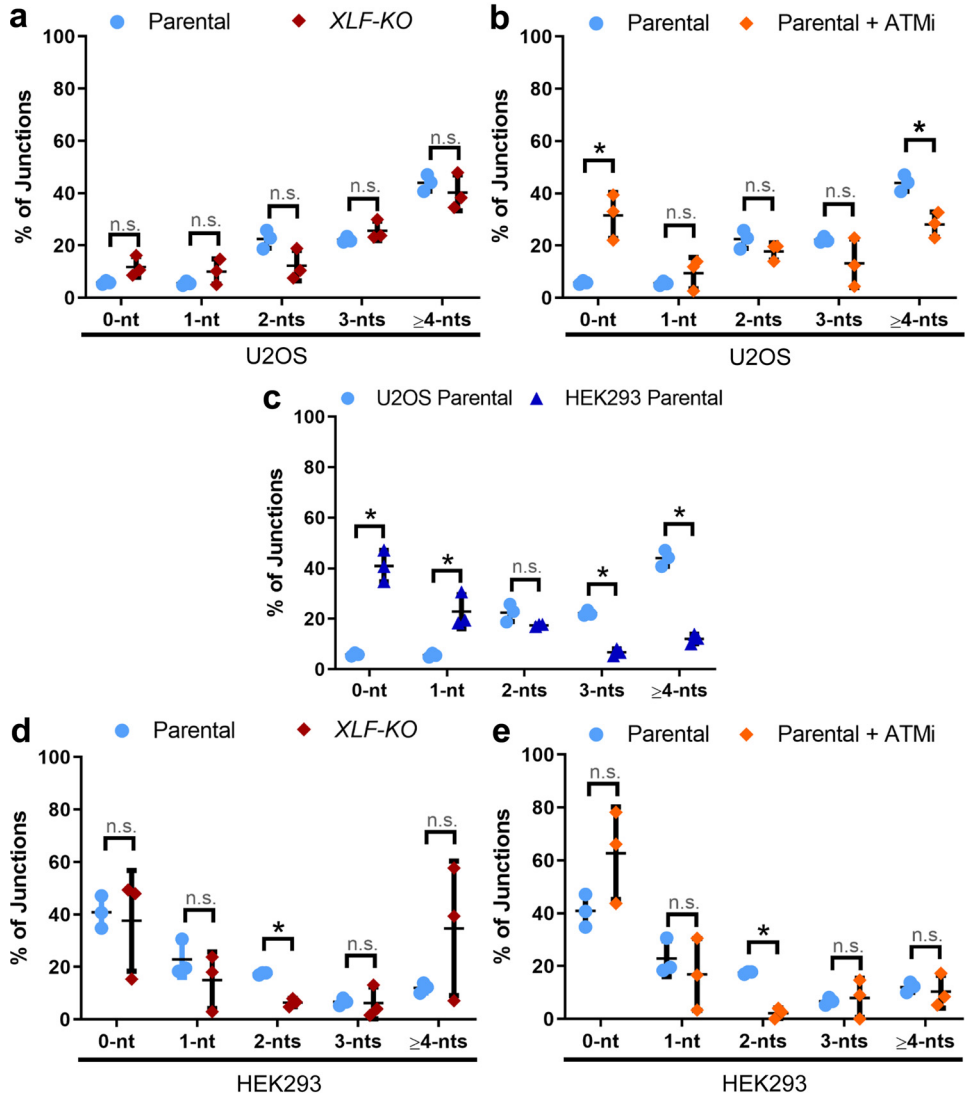

Figure 4. Microhomology at deletion rearrangement junctions in U2OS and HEK293 cells, along with effects of XLF-deficiency and ATMi treatment. *a*, microhomology use in U2OS parental *versus* U2OS *XLF-KO*. From the experiments in Fig. 3, sequences that represented ≥0.25% of total deletions and complex junctions were isolated and analyzed for microhomology. From these sequences, shown are the percentage junctions with 0, 1, 2, 3, and ≥4 nt of microhomology. As in Fig. 3, $n = 3$ independent biological replicates, *n.s.*, not significant. Shown is the mean with S.D. *b*, microhomology use in U2OS parental (DMSO) *versus* ATMi (KU-55933). Analysis as in (*a*), *, $p < 0.04$, *n.s.*, not significant, using an unpaired *t* test with Holm-Sidak correction. *c*, microhomology use in U2OS parental *versus* HEK293 parental. Analysis as in (*a*), statistics as in (*b*). *d*, microhomology use in HEK293 parental *versus* HEK293 *XLF-KO*. Analysis as in (*a*), statistics as in (*b*). *e*, microhomology use in HEK293 parental (DMSO) *versus* ATMi. Analysis as in (*a*), statistics as in (*b*). As in Fig. 3, the U2OS and HEK293 parental junctions are repeated in the different panels to facilitate the various comparisons.

microhomology to complex deletion mutations with insertions, or for simple insertions, because the sequence of the inserted nucleotides prior to ligation is unknown. From the analysis of simple deletions, we found that junctions from U2OS cells rarely exhibited events that utilized 0 nt (5.8%) or 1 nt of microhomology (5.5%), whereas events with 2, 3, and ≥4 nt of microhomology were more prevalent (22.4, 22.2, and 43%, respectively) (Fig. 4*a*). Interestingly, XLF loss does not affect the spectrum of microhomology use in U2OS cells (Fig. 4*a*). Conversely, ATMi treatment in U2OS cells caused an increase in deletions with no microhomology (0 nt, 31%, 5.4-fold higher), and a decrease in the use of ≥4 nt of microhomology (28%, 1.6-fold lower) (Fig. 4*b*).

Compared with U2OS cells, we found that HEK293 cells exhibited a bias toward junctions with simple deletions with 0 to 1 nt of microhomology (40.9 and 22.9%, respectively, 7- and 4.1-fold higher than U2OS cells, respectively) (Fig. 4*c*) and a decrease in junctions with 3 and ≥4 nt of microhomology (6.7 and 12.1%, respectively, 3.3- and 3.6-fold lower than U2OS cells, respectively) (Fig. 4*c*). Finally, HEK293 *XLF-KO* cells, as well as HEK293 parental cells treated with ATMi, showed minor changes in the use of microhomology at the junctions (*i.e.* a decrease in 2 nt of microhomology, compared with parental cells) (Fig. 4, *d* and *e*, respectively). In summary, junctions without microhomology were rare for U2OS cells, but prevalent for U2OS cells treated with ATMi, and for HEK293 cells.

Given that we observed differences in the junction patterns, and effects of ATMi treatment, between U2OS and HEK293 cells, we next sought to examine a third cell type. Specifically, we used the A549 lung cancer cell line, because we found that the *GAPDH-CD4* rearrangement assay is feasible in these cells (Fig. 1*c*). We also chose A549 cells as a means to evaluate a

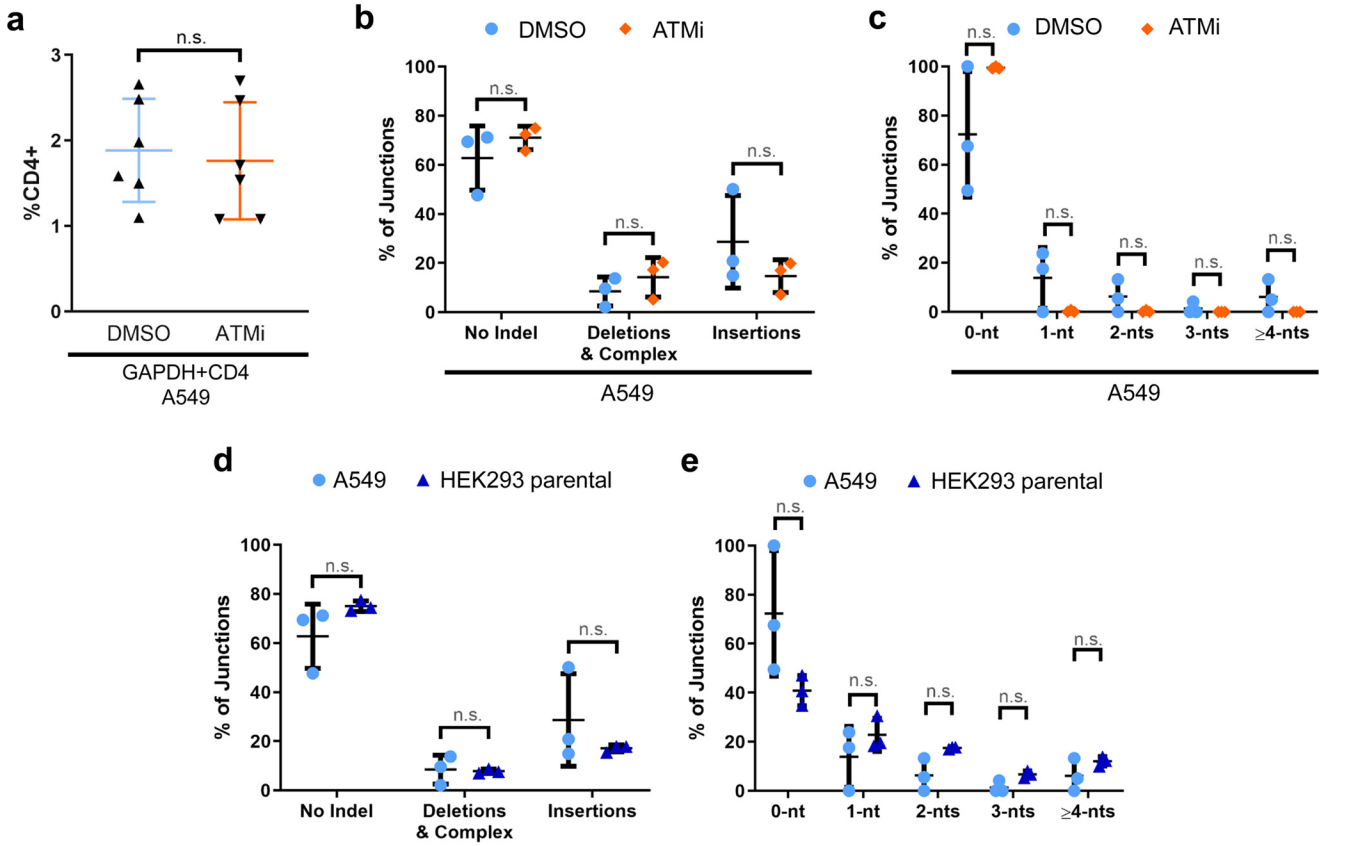

Figure 5. Deletion rearrangement frequencies and junction patterns for A549 cells with and without ATMi treatment. *a*, shown is the percentage of CD4+ cells in A549 cells transfected with the GAPDH and CD4 sgRNA/Cas9 expression vectors in the presence of either the ATMi (KU-55933) or vehicle (DMSO), normalized to transfection efficiency as in Fig. 1*c*. Shown is the mean with S.D.; n.s., not significant. *b*, shown are indel junction types for the *GAPDH–CD4* rearrangement for A549 cells treated with ATMi (KU-55933) or vehicle (DMSO), using the categories in Fig. 3*b*. $n = 3$ amplicons from independent biological replicates. Shown is the mean with S.D.; *n.s.*, not significant., using an unpaired *t* test with Holm-Sidak correction. *c*, shown is microhomology use for the A549 experiment shown in (*b*), which was analyzed as in Fig. 4*a*. Statistics as in (*b*). *d*, shown is a comparison of the indel junction types for the DMSO-treated samples for A549 cells in (*b*) *versus* HEK293 cells in Fig. 3*d*. Statistics as in (*b*). *e*, shown is a comparison of microhomology usage for the DMSO-treated samples for A549 cells in (*c*) *versus* HEK293 cells in Fig. 4*c*. Statistics as in (*b*).

second cancer cell line, in addition to U2OS. First, we examined whether ATMi treatment affected the frequency of the *GAPDH-CD4* rearrangement in A549 cells, and found that such treatment had no obvious effect (Fig. 5*a*). This finding is similar to our observations with HEK293 cells (Fig. 2*b*).

We then examined deletion rearrangement junctions for A549 cells that were either treated with ATMi or vehicle (DMSO). Namely, we performed amplicon deep sequencing analysis on CD4+ cells isolated by cell sorting, as described above. From this analysis, we found that A549 cells showed an average of 62.8% No Indel, 28.7% insertions, and 8.5% deletions and complex junctions (Fig. 5*b*). From microhomology analysis of the simple deletions, we found that events with 0 nt of microhomology were predominant (72.3%), whereas the events with 1, 2, 3, and ≥4 nt of microhomology showed frequencies of 13.9, 6.3, 1.4, and 6.1%, respectively (Fig. 5*c*). For both junction type and microhomology usage, ATMi treatment did not cause a significant effect (Fig. 5, *b* and *c*). Notably, the frequencies of junction types and microhomology use for A549 cells are similar to HEK293 cells (Fig. 5, *d* and *e*). Altogether, these findings indicate that A549 cells show similar results as HEK293 cells, regarding junction patterns, and the lack of an effect of ATMi treatment on deletion rearrangement frequency.

An XLF residue critical for the interaction with XRCC4 is important for both No Indel EJ and rearrangement formation

The above findings indicate that XLF is important to promote deletion rearrangements in human cells, as well as the No Indel junction type. To further examine if these functions are interrelated, we tested whether disruption of key residues in XLF may affect both rearrangement formation and No Indel EJ. In particular, we examined the XLF-L115D mutation, which is in the N-terminal globular head domain and has been shown to block the interaction of XLF with the C-NHEJ factor XRCC4 (39, 47), which we confirmed using co-immunoprecipitation analysis in U2OS cells (Fig. 6*a*). We also examined the XLF-K160D mutation, which is predicted to weaken the XLF homodimer interface because of disruption of a predicted salt bridge between the monomers (26, 48).

We confirmed that these mutants are expressed using their N-terminal 3×FLAG immunotag (Fig. 6*b*) and examined their relative ability to promote rearrangements (*GAPDH–CD4* rearrangement assay) and No Indel EJ using the EJ7-GFP reporter assay (26). As above, the *GAPDH–CD4* rearrangement assay refers to co-expression of Cas9 with sgRNAs targeting *GAPDH* and *CD4* to induce the *GAPDH–CD4* rearrangement,

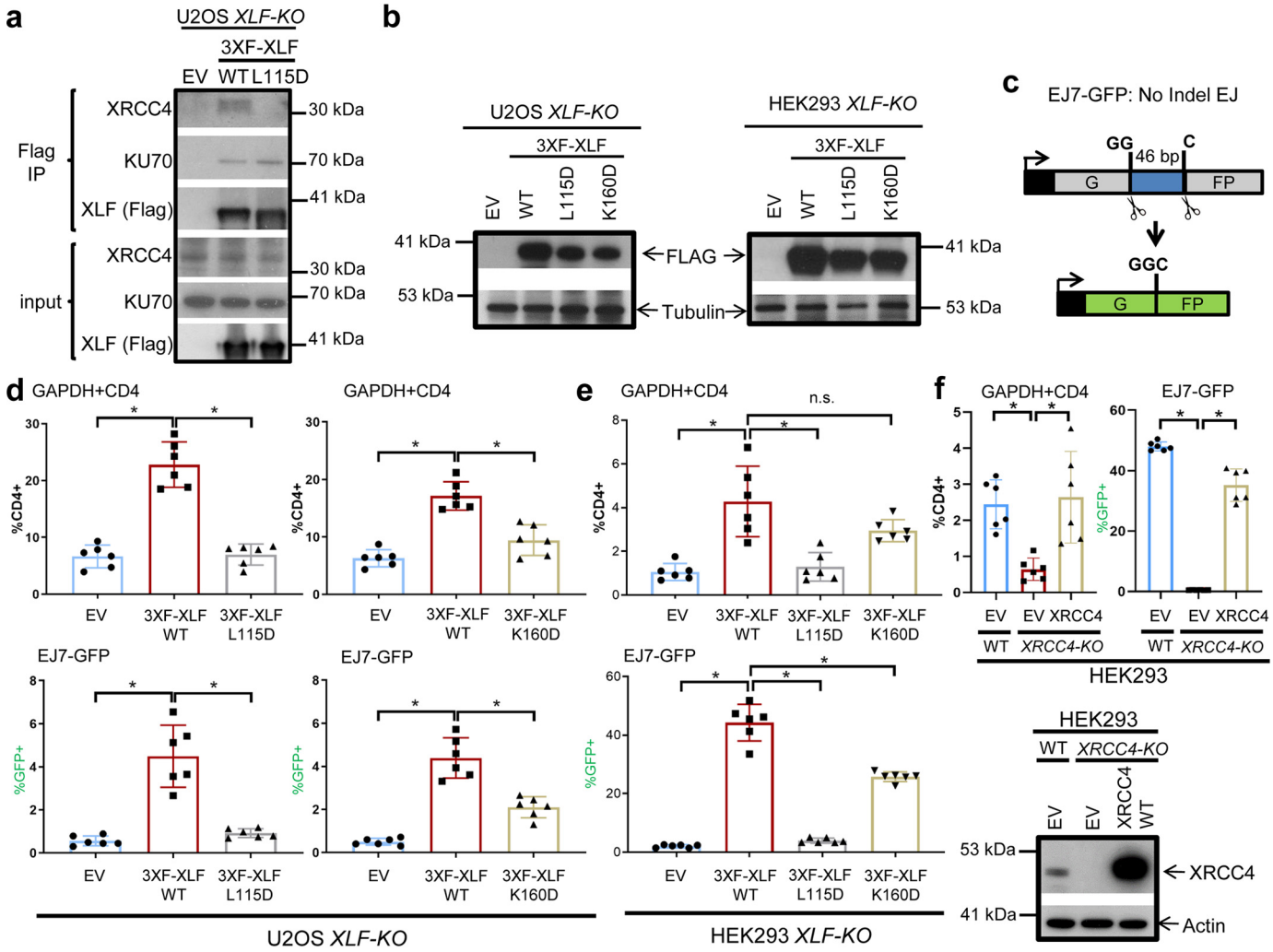

Figure 6. Disrupting the XLF-XRCC4 interaction (XLF-L115D) and loss of XRCC4 itself each cause defects in end joining without indels and rearrangement formation. *a*, shown is the effect of the XLF-L115D mutation on forming a co-immunoprecipitation complex with KU70 and XRCC4. Lysates were prepared from U2OS *XLF-KO* cells transfected with a control EV, or 3XF-XLF WT and L115D expression vectors. A fraction of the lysate was used to examine the proteins in the input, and the rest was used for a FLAG-immunoprecipitation (FLAG-IP). Shown are immunoblot signals for input and FLAG-IP samples for FLAG (XLF), KU70, and XRCC4. *b*, shown are FLAG immunoblots confirming expression of 3XF-XLF WT, L115D, and K160D in U2OS *XLF-KO* (*left*) and HEK293 *XLF-KO* (*right*) cells, with tubulin loading control. *c*, shown is a schematic of the EJ7-GFP assay for end joining without insertion/deletion mutations (*i.e.* No Indel EJ). *d*, analysis of XLF mutants in U2OS *XLF-KO* cells. For the *GAPDH-CD4* rearrangement assay, cells were transfected with Cas9 and sgRNAs targeting *GAPDH* and *CD4* (GAPDH plus CD4), as in Fig. 1*c*, along with either a control EV, a 3XF-XLF WT, or a mutant (L115D or K160D) expression vector. Similarly, U2OS *XLF-KO* cells with the EJ7-GFP reporter were transfected with the Cas9/sgRNA vectors for this assay, along with the other vectors for complementation analysis. Shown are the frequencies of CD4+ cells for the *GAPDH-CD4* rearrangement assay (*top*) or GFP+ cells for the EJ7-GFP assay (*bottom*), normalized to transfection efficiency, as in Fig. 1*c*. $n = 6$. Shown is the mean with S.D. *, $p < 0.0005$, using an unpaired *t* test with Holm-Sidak correction. *e*, analysis of XLF mutants in HEK293 *XLF-KO* cells. Shown are repair frequencies for the *GAPDH-CD4* rearrangement and EJ7-GFP assays, as in (*d*). *, $p < 0.004$, *n.s.*, not significant. *f*, analysis of an *XRCC4-KO* HEK293 cell line. Shown are repair frequencies for the *GAPDH–CD4* rearrangement and EJ7-GFP assays, following transfecting cells with the Cas9/sgRNA plasmids as in (*d*), along with either control EV, or an expression vector for XRCC4. $n = 6$, *, $p < 0.004$. Also shown is XRCC4 immunoblot analysis, with actin loading control, of the *XRCC4-KO* cell line transfected with EV or XRCC4 expression vector, and the parental HEK293 cells transfected with EV.

and subsequently quantifying the frequency of CD4+ cells, as in Fig. 1*c*. In the EJ7-GFP reporter, the GFP coding sequence has been disrupted by inserting a 46-nt spacer between the first two bases (GG) and the final base (C) of the codon for glycine 67 (Fig. 6*c*). We use sgRNAs to target two Cas9-induced DSBs to precisely excise the 46-nt spacer, such that No Indel EJ between the distal DSBs restores the GGC codon, and hence GFP+ expression. The EJ7-GFP reporter was integrated into cells using the Flp/FRT system (26).

From these experiments in both U2OS and HEK293 cells, we found that the XLF-L115D mutant showed a marked defect in promoting both the *GAPDH–CD4* rearrangement, as well as No Indel EJ using the EJ7-GFP assay, compared with XLF WT (Fig. 6, *d* and *e*). Similarly, the XLF-K160D mutant showed a significant defect in promoting these EJ events, but retained partial activity, and indeed for HEK293 cells with the *GAPDH–CD4* rearrangement assay, this mutant was not statistically significantly different from XLF WT (Fig. 6*e*). These findings indicate that a residue of XLF that is critical for the interaction with XRCC4 is important for both deletion rearrangements, as well as No Indel EJ.

Based on these findings with the XLF-L115D mutant, we posited that XRCC4 itself is critical for these EJ events. To test this hypothesis, we used Cas9 and sgRNAs targeting *XRCC4* to disrupt the *XRCC4* gene in the HEK293 EJ7-GFP cell line (*XRCC4-KO* cell line) (Fig. 6*f*). Using this cell line, we examined

the frequency of the *GAPDH–CD4* rearrangement, as well as No Indel EJ using the EJ7-GFP assay. From these experiments, we found that loss of XRCC4 caused a reduction in both the *GAPDH–CD4* rearrangement, and No Indel EJ, compared with the parental HEK293 cell line (Fig. 6*f*). Furthermore, expression of XRCC4 in the *XRCC4-KO* cell line caused a significant increase in these EJ events (Fig. 6*f*). These findings indicate that XRCC4 promotes the deletion measured by the *GAPDH–CD4* rearrangement assay, as well as No Indel EJ.

Discussion

Defining the mechanisms of DSB-induced chromosomal rearrangements provides insight into cancer etiology, as well as the consequences of clastogen exposure to genome stability. Here, we have described an assay to examine such rearrangements in human cells using the *CD4* gene and flanking promoters in the *GAPDH* and *LPCAT3* genes. Because these genes are already present on chromosome 12 (*i.e.* are endogenous to this chromosome), this assay has the potential to be versatile across human cells that do not already express CD4. Indeed, we have confirmed that this assay is robust in four different human cell lines. Thus, this assay could be used to examine the role of individual genes and small molecules on the frequency of chromosomal rearrangements in multiple cell types. Furthermore, in addition to frequency measurements, isolation of CD4+ cells enables the analysis of repair junction patterns, which can provide insight into the relative contribution of C-NHEJ to rearrangements.

Nonetheless, certain limitations of this assay should be considered. For one, the four cell lines tested here are readily transfected with simple lipofection, whereas other means of introducing the sgRNAs/Cas9 may be necessary for other cell types (*e.g.* nucleofection or viral transduction). Additionally, we found that these four cell lines showed very low background affinity for the phycoerythrin–CD4 antibody, whereas this assay is likely not feasible for cell lines with higher background staining. Furthermore, we found that an sgRNA targeting Cas9 to the *CD4* gene alone is able to induce CD4+ cells, albeit at a low level. The mechanism of such expression of CD4 is unclear. Nevertheless, the frequency of this event is much lower than for the *GAPDH–CD4* rearrangement, and hence does not appear to interfere with examining the frequency of this rearrangement. In any case, to adapt this approach to other cell lines, it will be critical to include analysis of the sgRNA targeting CD4 alone (see Fig. 1, *b* and *c*). Along these lines, although targeting DSBs to LPCAT3 and CD4 in U2OS cells induced CD4+ cells at a substantially higher frequency, compared with targeting a DSB to CD4 alone, the *LPCAT3–CD4* inversion events are lower than for the *GAPDH–CD4* deletion rearrangement. Thus, the *GAPDH–CD4* rearrangement assay is more robust, and hence was the focus of our mechanistic studies.

With the *GAPDH–CD4* rearrangement assay, we sought to examine the relative contribution of the C-NHEJ pathway to rearrangements in two cell types commonly used for studies of the DNA damage response (*i.e.* U2OS and HEK293). The relative contribution of C-NHEJ to rearrangement formation has been shown to vary among cell lines, but the primary focus has been on comparing mouse *versus* human cells. Namely, C-NHEJ appears dispensable for chromosomal translocations in mESCs, but was shown to promote translocations in a set of human cell lines (23, 24). Consistent with this notion, in a prior study, our laboratory found that the C-NHEJ factor XLF is dispensable for a 0.4-Mbp deletion rearrangement in mESCs (25), whereas here we found that XLF promotes the *GAPDH–CD4* rearrangement in both U2OS and HEK293 cells.

XLF not only promoted a higher frequency of this deletion rearrangement, but also was critical for the No Indel junction type in both U2OS and HEK293 cells. Other studies also support the notion that C-NHEJ factors are critical for No Indel EJ events (25, 49, 50), including a study with the EJ7-GFP assay used here (26). Indeed, we found that an XLF mutation that disrupts the interaction with XRCC4 (*i.e.* L115D), as well as loss of XRCC4 itself, each cause a reduction in both the *GAPDH–CD4* rearrangement and No Indel EJ (EJ7-GFP assay), indicating that these EJ events rely on similar mechanisms. Consistent with a key role for this XLF residue in EJ, the XLF-L115D mutant has also been shown to be defective in promoting resistance to the clastogen Zeocin (51). In addition to L115D, we found similar results with a mutation that disrupts the XLF dimer interface (K160D), although the effects were more modest, and not significant for the *GAPDH–CD4* rearrangement in HEK293 cells. Altogether, these findings support recent studies that XLF is a key stabilizing factor for the C-NHEJ complex and bridging DNA ends (39, 47).

However, although XLF promotes the deletion rearrangement in both U2OS and HEK293 cells, from junction analysis, C-NHEJ rearrangements appear less frequent in U2OS cells. Specifically, three different junctions types that appear mediated by C-NHEJ were lower in U2OS cells: No Indel junctions, insertion mutations, and deletion mutations without microhomology. Each of these EJ events are likely dependent on C-NHEJ, as they involve ligation without an annealing intermediate to stabilize the junction (11). Consistent with this notion, the No Indel junction depends on XLF, as described above, and similarly insertions are also promoted by XLF. Deletion mutations without microhomology have been shown to be dependent on C-NHEJ in several studies (17, 29), although we did not observe an obvious effect of XLF on microhomology use in this study, indicating a potential redundancy for XLF for such EJ events.

The mechanisms that underlie this difference in junction patterns between U2OS and HEK293 cells are unclear. Indeed, there are several possibilities, because the origins of these cell lines are very distinct (*e.g.* osteosarcoma cells *versus* an adenovirus immortalized kidney cell line, respectively) (36, 52). Furthermore, the junction patterns for the HEK293 cell line appear similar to those of the A549 lung cancer cell line. Notably, U2OS cells treated with an ATM kinase inhibitor (*i.e.* ATMi) show similar junctions patterns as HEK293 and A549 cells. Namely, U2OS cells treated with ATMi showed a high frequency of the No Indel junction, which was similar to that of HEK293 and A549 cells. ATMi treatment of U2OS cells also caused an overall higher frequency of the *GAPDH–CD4* rearrangement, in a manner dependent on XLF. These effects of ATMi treatment are similar to a prior report from our laboratory on a deletion rearrangement in mESCs (25), as well as other

reports that ATM is important to limit toxic C-NHEJ events (53). Thus, a role of ATM kinase activity in suppressing C-NHEJ–mediated rearrangements appears to be conserved in mouse and human cells.

However, ATMi treatment did not have substantial effects on HEK293 and A549 cells, perhaps because these cells already show a high frequency of C-NHEJ–mediated rearrangements. Thus, we speculate that HEK293 and/or A549 cells could be deficient in some aspect of the ATM-mediated DNA damage response signaling that is important to suppress C-NHEJ rearrangements. Conversely, U2OS cells may be hyperactive for this aspect of ATM-mediated signaling. In any case, examining these possibilities will require further insight into the mechanisms by which ATM kinase signaling suppresses C-NHEJ rearrangements. We suggest that the assay systems described here provide a platform for such further mechanistic studies in multiple human cell lines.

Experimental procedures

Cell lines and plasmids

The following human cell lines were authenticated by short tandem-repeat profiling: HEK293 Flp-In T-REx (36), U2OS Flp-In T-REx (26, 30), and A549 (35). The GM00637 SV40 transformed human fibroblast cell line was acquired directly from the Coriell repository. The HEK293 and U2OS cells were cultured as described (54), and the same medium was used for A549 cells. GM00637 cells were cultured using minimum Eagle's medium supplemented with nonessential amino acids, 12.5% FBS, 1% penicillin/streptomycin, and 0.015% plasmocin (Invivogen). The EJ7-GFP reporter was integrated into the chromosomal FRT site of the HEK293 Flp-In T-REx cells, as previously described for the generation of the U2OS EJ7-GFP cell line (26).

For CAS9/sgRNA expression, the px330 plasmid was used (Addgene 42230) (55). These sgRNA sequences were used to target *GAPDH* (px330-GAPDH, 5′-GTATAGAAACCGGGGGCGCGG, the first G base is not in the target locus but is required for transcription of the sgRNA), *CD4* (px330-CD4, 5′-GGCGTATCTGTGTGAGGACT), and *LPCAT3* (px330-LPCAT3, 5′-GATAGCGTTTTGCCCGCATT). The pCAGGS-3×FLAG-XLF (human) and empty vector (EV, pCAGGS-BSKX) were described previously (26, 56) and used to generate the XLF mutants by inserting gBLOCK fragments (Integrated DNA Technologies). To generate the *XLF-KO* cell lines, an sgRNA sequence targeting XLF (5′-GTTGGTTTCAGATCTTCAAC) (40) was introduced into px330 (px330-XLF). To generate the HEK293 *XLF-KO* cell line, px330-XLF (200 ng) was co-transfected with pgk-puro (54) (60 ng) using 1.8 μl of Lipofectamine 2000 into the HEK293 EJ7-GFP cell line seeded on a 24-well plate. These cells were subsequently selected in puromycin (3 μg/ml) for 3 days and plated at low density without puromycin selection to isolate individual clones. For the U2OS cell line, px330-XLF (800 ng) was co-transfected into the U2OS Flp-In T-REx cell line with dsRED (150 ng) with 6 μl of Lipofectamine 2000 into cells seeded on a 6-well plate. Cells were subsequently sorted for dsRED expressing cells (ARIA sorter, BD Biosciences) and plated at low density to isolate individual clones. Clones were screened by immunoblotting (see below). The EJ7-GFP reporter was integrated into the U2OS *XLF-KO* cell line, as described above. This cell line was used only for the EJ7-GFP reporter analysis. To generate the HEK293 *XRCC4-KO* cell line, a similar procedure was used for creating the HEK293 *XLF-KO* cell line, as described above, except using two sgRNAs to target XRCC4, using these sequences cloned into px330: 5′-GATGACATGGCAATGGAAAA and 5′-GTTAAACGTGTATACATCAGC. Also, in this case, the transfection was scaled to a 12-well plate using 400 ng each px330 plasmid and 100 ng pgk-puro plasmid. The pCAGGS-XRCC4 expression vector was described previously (26). The 7a and 7b sgRNA/Cas9 plasmids for inducing DSBs in the EJ7-GFP reporter were described previously (26).

CD4 rearrangement and EJ7-GFP assays

Cells were seeded on a 24-well plate and subsequently transfected with 200 ng each of px330-GAPDH and px330-CD4, or px330-LPCAT3 and px330-CD4, along with 20 ng of EV or pCAGGS-3×FLAG-XLF expression vector (WT or mutant), with 1.8 μl Lipofectamine 2000 in a total of 0.6 ml. Transfections with one px330 plasmid included 220 ng of EV to maintain equivalent plasmid concentrations. Similarly, to determine transfection efficiency, 200 ng of GFP expression vector (pCAGGS-NZEGFP) (54) and 220 ng of EV were used. Experiments comparing HEK293 parental *versus XRCC4-KO* used 100 ng of EV or pCAGGS-XRCC4. The transfection mixes were removed after 4 h, the wells were washed with DMEM, and complete media was added either with 10 μM ATMi (KU-55933, Selleck Chemicals, S1092) (41), 5 μM ATMi-2 (KU-60019, Selleck Chemicals, S1570) (42), 10 μM DNAPKi (NU7441, Selleck Chemicals, S2638) (43), or vehicle (DMSO). ATMi and DMSO treatments were for 3 days, at which point the cells were processed for analysis or cultured in untreated media for subsequent isolation by cell sorting. For CD4 staining, cells were harvested, washed with PBS, incubated in 100 μl staining buffer (10% FBS, 1% sodium azide) with 2 μl phycoerythrin-CD4 antibody (BioLegend, 317410) for 20 min on ice, followed by three washes with staining buffer. For flow cytometry analysis, cells were fixed by mixing 200 μl cells in staining buffer with 90 μl 10% formaldehyde (*e.g.* VWR International, MKH12108) and then analyzed with a CyAn ADP cytometer (Dako). For isolation of CD4+ cells, the staining was performed as with the analysis using double the volume of staining buffer and antibody, but without sodium azide in the staining buffer and without fixation, and cells were sorted using an ARIA III or ARIA SORP (BD Biosciences). For isolation of CD4+ cells from A549 cells, the transfections were scaled 4-fold onto a 6-well plate. For the EJ7-GFP reporter, transfections were performed as for the CD4 assay, but using the 7a and 7b sgRNA/Cas9 plasmids and without DMSO or ATMi treatment. Analysis of GFP+ cells was performed as described (26).

Rearrangement junction analysis

Genomic DNA was isolated from CD4+ or control cells as described (54) and used for PCR amplification (Platinum HiFi Supermix, Thermo Fisher). Amplicons of the deletion rearrangement products were generated with primers P1 (5′-ctac-

tagcggttttacgggc-3′) and P2 (5′-ctgacctctggaagctcaca-3′). Control amplification of *RAD52* used these primers: 5′-aagtcccctcctttcctctg and 5′-ctcgctcaccctcactcttc. For sequencing library preparation, purified amplicons underwent two rounds of PCR. The first round of PCR used nested primers (5′-ctacacgacgctcttccgatctaagaccttgggctgggact and 5′-gtgactggagttcagacgtgtgctcttccgatctaccttacctctgggcttgc) with Illumina universal sequences and amplified for five cycles. The PCR products were purified with 1.0× Ampure XP Beads (BD Biosciences, A63882) and followed by the second round of PCR with the barcoded index primers and amplified for four cycles. The final purified libraries were validated with the Agilent Bioanalyzer DNA High Sensitivity DNA Kit (Agilent, 5067-4627) and quantified with Qubit and qPCR. The libraries were sequenced on Illumina HiSeq 2500 with HiSeq Rapid SBS Kit v2 in the paired end mode of 101 cycles of read1, 7 cycles of index read, and 101 cycles of read2. Real-time analysis 2.2.38 software was used to process the image analysis and base calling.

Paired-end amplicon reads of 2 × 101 bp were merged using PEAR (paired-end read merger v0.9.5), and the merged amplicon sequences were processed with customized scripts that tallied unique sequence and its occurrence in amplicons, aligned each unique sequence to the reference sequence with Novoalign (v3.02.07, Novocraft Technologies), and generated detailed information of mutation and indel using SAMtools (v0.1.19) and VarScan (v.2.3.9). The sequencing reads of each amplicon (>1.4 million reads per sample) were examined to determine the frequencies (*i.e.* percentage) of distinct junction categories. For each condition, such analysis from three biological replicates (*i.e.* amplicon deep sequencing from three independent transfections) was used to calculate the mean and S.D. for the frequencies of distinct junction categories.

Immunoprecipitation and immunoblotting

For immunoblot analysis, protein was extracted using NETN (20 mM Tris, pH 8, 100 mM NaCl, 1 mM EDTA, 0.5% IGEPAL, 1 mM DTT, and Roche Protease Inhibitor Mixture), and several freeze/thaw cycles. Blots of the protein gels were probed with the following antibodies for detection by Amersham ECL (GE Healthcare): XLF (Bethyl, A300–730A), HRP-conjugated FLAG (Sigma, A8592), XRCC4 (Santa Cruz Biotechnology, 271087, 271087 HRP), KU70 (Cell Signaling Technology, D10A7), tubulin (Sigma, T9026), and HRP-conjugated secondary antibodies (Abcam, 205718, 205719).

For each immunoprecipitation, 2 × 10^5 U2OS cells were seeded on two 10-cm plates, and each plate was transfected with 3 μg of 3×FLAG-XLF expression vector or EV with 12 μl of Lipofectamine 2000. Following 2 days after transfection, protein was extracted using NETN along with Dounce homogenization, followed by incubation with anti-FLAG M2 magnetic beads (Sigma, M8823) overnight at 4 °C. Beads were washed twice with NETN buffer, and proteins were eluted with 100 mM glycine (pH 2.5) and neutralized with 1 M Tris-HCl (pH 10.8).

Author contributions—R. B., F. W. L., L. J. T., and J. M. S. conceptualization; R. B., F. W. L., L. J. T., and J. M. S. resources; R. B., F. W. L., L. J. T., and J. M. S. investigation; R. B., F. W. L., L. J. T., and J. M. S. writing-review and editing; J. M. S. funding acquisition.

Acknowledgments—We thank Gabriella Lee, Shu Tao, Junhui Wang, and Xiwei Wu for technical assistance.

References

1. Iliakis, G. (1991) The role of DNA double strand breaks in ionizing radiation-induced killing of eukaryotic cells. *Bioessays* **13,** 641–648 CrossRef Medline
2. Mladenov, E., Magin, S., Soni, A., and Iliakis, G. (2013) DNA double-strand break repair as determinant of cellular radiosensitivity to killing and target in radiation therapy. *Front. Oncol.* **3,** 113 CrossRef Medline
3. Behjati, S., Gundem, G., Wedge, D. C., Roberts, N. D., Tarpey, P. S., Cooke, S. L., Van Loo, P., Alexandrov, L. B., Ramakrishna, M., Davies, H., Nik-Zainal, S., Hardy, C., Latimer, C., Raine, K. M., Stebbings, L., *et al.* (2016) Mutational signatures of ionizing radiation in second malignancies. *Nat. Commun.* **7,** 12605 CrossRef Medline
4. Hillman, R. T., Chisholm, G. B., Lu, K. H., and Futreal, P. A. (2018) Genomic rearrangement signatures and clinical outcomes in high-grade serous ovarian cancer. *J. Natl. Cancer Inst.* **110,** 265–272 CrossRef Medline
5. Nik-Zainal, S., Davies, H., Staaf, J., Ramakrishna, M., Glodzik, D., Zou, X., Martincorena, I., Alexandrov, L. B., Martin, S., Wedge, D. C., Van Loo, P., Ju, Y. S., Smid, M., Brinkman, A. B., Morganella, S., *et al.* (2016) Landscape of somatic mutations in 560 breast cancer whole-genome sequences. *Nature* **534,** 47–54 CrossRef Medline
6. Bignell, G. R., Greenman, C. D., Davies, H., Butler, A. P., Edkins, S., Andrews, J. M., Buck, G., Chen, L., Beare, D., Latimer, C., Widaa, S., Hinton, J., Fahey, C., Fu, B., Swamy, S., *et al.* (2010) Signatures of mutation and selection in the cancer genome. *Nature* **463,** 893–898 CrossRef Medline
7. Stephens, P. J., McBride, D. J., Lin, M.-L., Varela, I., Pleasance, E. D., Simpson, J. T., Stebbings, L. A., Leroy, C., Edkins, S., Mudie, L. J., Greenman, C. D., Jia, M., Latimer, C., Teague, J. W., Lau, K. W., *et al.* (2009) Complex landscapes of somatic rearrangement in human breast cancer genomes. *Nature* **462,** 1005–1010 CrossRef Medline
8. Le, Q. T., Shirato, H., Giaccia, A. J., and Koong, A. C. (2015) Emerging treatment paradigms in radiation oncology. *Clin. Cancer Res.* **21,** 3393–3401 CrossRef Medline
9. Sallmyr, A., and Tomkinson, A. E. (2018) Repair of DNA double-strand breaks by mammalian alternative end-joining pathways. *J. Biol. Chem.* **293,** 10536–10546 CrossRef Medline
10. Ochi, T., Wu, Q., and Blundell, T. L. (2014) The spatial organization of non-homologous end joining: From bridging to end joining. *DNA Repair* **17,** 98–109 CrossRef Medline
11. Chang, H. H. Y., Pannunzio, N. R., Adachi, N., and Lieber, M. R. (2017) Non-homologous DNA end joining and alternative pathways to double-strand break repair. *Nat. Rev. Mol. Cell Biol.* **18,** 495–506 CrossRef Medline
12. Radhakrishnan, S. K., Jette, N., and Lees-Miller, S. P. (2014) Non-homologous end joining: Emerging themes and unanswered questions. *DNA Repair* **17,** 2–8 CrossRef Medline
13. Beagan, K., and McVey, M. (2016) Linking DNA polymerase theta structure and function in health and disease. *Cell Mol. Life Sci.* **73,** 603–615 CrossRef Medline
14. Seol, J. H., Shim, E. Y., and Lee, S. E. (2018) Microhomology-mediated end joining: Good, bad and ugly. *Mutat. Res.* **809,** 81–87 CrossRef Medline
15. Wyatt, D. W., Feng, W., Conlin, M. P., Yousefzadeh, M. J., Roberts, S. A., Mieczkowski, P., Wood, R. D., Gupta, G. P., and Ramsden, D. A. (2016) Essential roles for polymerase theta-mediated end joining in the repair of chromosome breaks. *Mol. Cell* **63,** 662–673 CrossRef Medline
16. Howard, S. M., Yanez, D. A., and Stark, J. M. (2015) DNA damage response factors from diverse pathways, including DNA crosslink repair, mediate alternative end joining. *PLoS Genet.* **11,** e1004943 CrossRef Medline
17. Guirouilh-Barbat, J., Rass, E., Plo, I., Bertrand, P., and Lopez, B. S. (2007) Defects in XRCC4 and KU80 differentially affect the joining of distal nonhomologous ends. *Proc. Natl. Acad. Sci. U.S.A.* **104,** 20902–20907 CrossRef Medline

18. Haber, J. E. (2008) Alternative endings. *Proc. Natl. Acad. Sci. U.S.A.* **105,** 405–406 CrossRef Medline
19. Bennardo, N., Cheng, A., Huang, N., and Stark, J. M. (2008) Alternative-NHEJ is a mechanistically distinct pathway of mammalian chromosome break repair. *PLoS Genet.* **4,** e1000110 CrossRef Medline
20. Zhu, C., Mills, K. D., Ferguson, D. O., Lee, C., Manis, J., Fleming, J., Gao, Y., Morton, C. C., and Alt, F. W. (2002) Unrepaired DNA breaks in p53-deficient cells lead to oncogenic gene amplification subsequent to translocations. *Cell* **109,** 811–821 CrossRef Medline
21. Schimmel, J., Kool, H., van Schendel, R., and Tijsterman, M. (2017) Mutational signatures of non-homologous and polymerase theta-mediated end-joining in embryonic stem cells. *EMBO J.* **36,** 3634–3649 CrossRef Medline
22. Pannunzio, N. R., Li, S., Watanabe, G., and Lieber, M. R. (2014) Non-homologous end joining often uses microhomology: Implications for alternative end joining. *DNA Repair* **17,** 74–80 CrossRef Medline
23. Simsek, D., and Jasin, M. (2010) Alternative end-joining is suppressed by the canonical NHEJ component Xrcc4-ligase IV during chromosomal translocation formation. *Nat. Struct. Mol. Biol.* **17,** 410–416 CrossRef Medline
24. Ghezraoui, H., Piganeau, M., Renouf, B., Renaud, J. B., Sallmyr, A., Ruis, B., Oh, S., Tomkinson, A. E., Hendrickson, E. A., Giovannangeli, C., Jasin, M., and Brunet, E. (2014) Chromosomal translocations in human cells are generated by canonical nonhomologous end-joining. *Mol. Cell* **55,** 829–842 CrossRef Medline
25. Bhargava, R., Carson, C. R., Lee, G., and Stark, J. M. (2017) Contribution of canonical nonhomologous end joining to chromosomal rearrangements is enhanced by ATM kinase deficiency. *Proc. Natl. Acad. Sci. U.S.A.* **114,** 728–733 CrossRef Medline
26. Bhargava, R., Sandhu, M., Muk, S., Lee, G., Vaidehi, N., and Stark, J. M. (2018) C-NHEJ without indels is robust and requires synergistic function of distinct XLF domains. *Nature Commun.* **9,** 2484 CrossRef Medline
27. Fagerberg, L., Hallström, B. M., Oksvold, P., Kampf, C., Djureinovic, D., Odeberg, J., Habuka, M., Tahmasebpoor, S., Danielsson, A., Edlund, K., Asplund, A., Sjöstedt, E., Lundberg, E., Szigyarto, C. A., Skogs, M., *et al.* (2014) Analysis of the human tissue-specific expression by genome-wide integration of transcriptomics and antibody-based proteomics. *Mol. Cell. Proteomics* **13,** 397–406 CrossRef Medline
28. Salmon, P., Giovane, A., Wasylyk, B., and Klatzmann, D. (1993) Characterization of the human CD4 gene promoter: Transcription from the CD4 gene core promoter is tissue-specific and is activated by Ets proteins. *Proc. Natl. Acad. Sci. U.S.A.* **90,** 7739–7743 CrossRef Medline
29. Guirouilh-Barbat, J., Huck, S., Bertrand, P., Pirzio, L., Desmaze, C., Sabatier, L., and Lopez, B. S. (2004) Impact of the KU80 pathway on NHEJ-induced genome rearrangements in mammalian cells. *Mol. Cell* **14,** 611–623 CrossRef Medline
30. Zhou, Y., Lee, J. H., Jiang, W., Crowe, J. L., Zha, S., and Paull, T. T. (2017) Regulation of the DNA damage response by DNA-PKcs inhibitory phosphorylation of ATM. *Mol. Cell* **65,** 91–104 CrossRef Medline
31. Cotta-Ramusino, C., McDonald, E. R., 3rd, Hurov, K., Sowa, M. E., Harper, J. W., and Elledge, S. J. (2011) A DNA damage response screen identifies RHINO, a 9–1-1 and TopBP1 interacting protein required for ATR signaling. *Science* **332,** 1313–1317 CrossRef Medline
32. Nghiem, P., Park, P. K., Kim, Y., Vaziri, C., and Schreiber, S. L. (2001) ATR inhibition selectively sensitizes G_1 checkpoint-deficient cells to lethal premature chromatin condensation. *Proc. Natl. Acad. Sci. U.S.A.* **98,** 9092–9097 CrossRef Medline
33. Lovejoy, C. A., Li, W., Reisenweber, S., Thongthip, S., Bruno, J., de Lange, T., De, S., Petrini, J. H., Sung, P. A., Jasin, M., Rosenbluh, J., Zwang, Y., Weir, B. A., Hatton, C., Ivanova, E., *et al.* (2012) Loss of ATRX, genome instability, and an altered DNA damage response are hallmarks of the alternative lengthening of telomeres pathway. *PLoS Genet.* **8,** e1002772 CrossRef Medline
34. Bayani, J., Zielenska, M., Pandita, A., Al-Romaih, K., Karaskova, J., Harrison, K., Bridge, J. A., Sorensen, P., Thorner, P., and Squire, J. A. (2003) Spectral karyotyping identifies recurrent complex rearrangements of chromosomes 8, 17, and 20 in osteosarcomas. *Genes Chromosomes Cancer* **36,** 7–16 CrossRef Medline
35. Giard, D. J., Aaronson, S. A., Todaro, G. J., Arnstein, P., Kersey, J. H., Dosik, H., and Parks, W. P. (1973) *In vitro* cultivation of human tumors: Establishment of cell lines derived from a series of solid tumors. *J. Natl. Cancer Inst.* **51,** 1417–1423 CrossRef Medline
36. Lin, Y. C., Boone, M., Meuris, L., Lemmens, I., Van Roy, N., Soete, A., Reumers, J., Moisse, M., Plaisance, S., Drmanac, R., Chen, J., Speleman, F., Lambrechts, D., Van de Peer, Y., Tavernier, J., and Callewaert, N. (2014) Genome dynamics of the human embryonic kidney 293 lineage in response to cell biology manipulations. *Nat. Commun.* **5,** 4767 CrossRef Medline
37. Frit, P., Ropars, V., Modesti, M., Charbonnier, J. B., and Calsou, P. (2019) Plugged into the Ku-DNA hub: The NHEJ network. *Prog. Biophys. Mol. Biol.* **147,** 62–76 CrossRef Medline
38. Brouwer, I., Sitters, G., Candelli, A., Heerema, S. J., Heller, I., de Melo, A. J., Zhang, H., Normanno, D., Modesti, M., Peterman, E. J., and Wuite, G. J. (2016) Sliding sleeves of XRCC4-XLF bridge DNA and connect fragments of broken DNA. *Nature* **535,** 566–569 CrossRef Medline
39. Graham, T. G. W., Carney, S. M., Walter, J. C., and Loparo, J. J. (2018) A single XLF dimer bridges DNA ends during nonhomologous end joining. *Nat. Struct. Mol. Biol.* **25,** 877–884 CrossRef Medline
40. Tadi, S. K., Tellier-Lebègue, C., Nemoz, C., Drevet, P., Audebert, S., Roy, S., Meek, K., Charbonnier, J. B., and Modesti, M. (2016) PAXX is an accessory c-NHEJ factor that associates with Ku70 and has overlapping functions with XLF. *Cell Rep.* **17,** 541–555 CrossRef Medline
41. Hickson, I., Zhao, Y., Richardson, C. J., Green, S. J., Martin, N. M. B., Orr, A. I., Reaper, P. M., Jackson, S. P., Curtin, N. J., and Smith, G. C. M. (2004) Identification and characterization of a novel and specific inhibitor of the ataxia-telangiectasia mutated kinase ATM. *Cancer Res.* **64,** 9152–9159 CrossRef Medline
42. Golding, S. E., Rosenberg, E., Valerie, N., Hussaini, I., Frigerio, M., Cockcroft, X. F., Chong, W. Y., Hummersone, M., Rigoreau, L., Menear, K. A., O'Connor, M. J., Povirk, L. F., van Meter, T., and Valerie, K. (2009) Improved ATM kinase inhibitor KU-60019 radiosensitizes glioma cells, compromises insulin, AKT and ERK prosurvival signaling, and inhibits migration and invasion. *Mol. Cancer Ther.* **8,** 2894–2902 CrossRef Medline
43. Leahy, J. J., Golding, B. T., Griffin, R. J., Hardcastle, I. R., Richardson, C., Rigoreau, L., and Smith, G. C. (2004) Identification of a highly potent and selective DNA-dependent protein kinase (DNA-PK) inhibitor (NU7441) by screening of chromenone libraries. *Bioorg. Med. Chem. Lett.* **14,** 6083–6087 CrossRef Medline
44. Lovejoy, C. A., and Cortez, D. (2009) Common mechanisms of PIKK regulation. *DNA Repair* **8,** 1004–1008 CrossRef Medline
45. Meek, K., Dang, V., and Lees-Miller, S. P. (2008) DNA-PK: The means to justify the ends? *Adv. Immunol.* **99,** 33–58 CrossRef Medline
46. Jiang, W., Crowe, J. L., Liu, X., Nakajima, S., Wang, Y., Li, C., Lee, B. J., Dubois, R. L., Liu, C., Yu, X., Lan, L., and Zha, S. (2015) Differential phosphorylation of DNA-PKcs regulates the interplay between end-processing and end-ligation during nonhomologous end-joining. *Mol. Cell* **58,** 172–185 CrossRef Medline
47. Normanno, D., Negrel, A., de Melo, A. J., Betzi, S., Meek, K., and Modesti, M. (2017) Mutational phospho-mimicry reveals a regulatory role for the XRCC4 and XLF C-terminal tails in modulating DNA bridging during classical non-homologous end joining. *Elife* **6,** e22900 CrossRef Medline
48. Li, Y., Chirgadze, D. Y., Bolanos-Garcia, V. M., Sibanda, B. L., Davies, O. R., Ahnesorg, P., Jackson, S. P., and Blundell, T. L. (2008) Crystal structure of human XLF/Cernunnos reveals unexpected differences from XRCC4 with implications for NHEJ. *EMBO J.* **27,** 290–300 CrossRef Medline
49. Guo, T., Feng, Y. L., Xiao, J. J., Liu, Q., Sun, X. N., Xiang, J. F., Kong, N., Liu, S. C., Chen, G. Q., Wang, Y., Dong, M. M., Cai, Z., Lin, H., Cai, X. J., and Xie, A. Y. (2018) Harnessing accurate non-homologous end joining for efficient precise deletion in CRISPR/Cas9-mediated genome editing. *Genome Biol.* **19,** 170 CrossRef Medline
50. Shou, J., Li, J., Liu, Y., and Wu, Q. (2018) Precise and predictable CRISPR chromosomal rearrangements reveal principles of Cas9-mediated nucleotide insertion. *Mol. Cell* **71,** 498–509.e4 CrossRef Medline
51. Roy, S., de Melo, A. J., Xu, Y., Tadi, S. K., Négrel, A., Hendrickson, E., Modesti, M., and Meek, K. (2015) XRCC4/XLF interaction is variably

required for DNA repair and is not required for ligase IV stimulation. *Mol. Cell. Biol.* **35,** 3017–3028 CrossRef Medline

52. Pontén, J., and Saksela, E. (1967) Two established in vitro cell lines from human mesenchymal tumours. *Int. J. Cancer* **2,** 434–447 CrossRef Medline
53. Balmus, G., Barros, A. C., Wijnhoven, P. W., Lescale, C., Hasse, H. L., Boroviak, K., le Sage, C., Doe, B., Speak, A. O., Galli, A., Jacobsen, M., Deriano, L., Adams, D. J., Blackford, A. N., and Jackson, S. P. (2016) Synthetic lethality between PAXX and XLF in mammalian development. *Genes Dev.* **30,** 2152–2157 CrossRef Medline
54. Gunn, A., and Stark, J. M. (2012) I-SceI-based assays to examine distinct repair outcomes of mammalian chromosomal double strand breaks. *Methods Mol. Biol.* **920,** 379–391 CrossRef Medline
55. Ran, F. A., Hsu, P. D., Wright, J., Agarwala, V., Scott, D. A., and Zhang, F. (2013) Genome engineering using the CRISPR-Cas9 system. *Nat. Protoc.* **8,** 2281–2308 CrossRef Medline
56. Stark, J. M., Pierce, A. J., Oh, J., Pastink, A., and Jasin, M. (2004) Genetic steps of mammalian homologous repair with distinct mutagenic consequences. *Mol. Cell. Biol.* **24,** 9305–9316 CrossRef Medline